Title
MORPHOLOGICAL EVOLUTION OF PORE CHANNELS IN ALUMINA

Authors
Rodel, J.
Glaeser, A.M.

Publication Date
1988-08-01

Lawrence Berkeley Laboratory
UNIVERSITY OF CALIFORNIA

Materials & Chemical Sciences Division

Presented at the International Symposium on
Processing of Advanced Ceramics, Cincinnati, OH,
May 1–5, 1988, and to be published in the Proceedings

Morphological Evolution of Pore Channels in Alumina

J. Rödel and A.M. Glaeser

August 1988

Prepared for the U.S. Department of Energy under Contract Number DE-AC03-76SF00098.

DISCLAIMER

ACS Conference Symposium Proceedings LBL Report #25147

Morphological Evolution of Pore Channels in Alumina

by

J. Rödel and A. M. Glaeser

Department of Materials Science and Mineral Engineering and
Materials and Chemical Sciences Division
Lawrence Berkeley Laboratory
University of California
Berkeley, California 94720

Abstract:

The morphological evolution of pore channels in sapphire bicrystals during annealing at 1800°C has been studied. The effects of boundary crystallography as well as channel orientation within the boundary plane have been examined by using bicrystals with channels etched into either the (0001) or the $(11\bar{2}0)$ planes, and oriented parallel to the $[1\bar{1}00]$ and $[11\bar{2}0]$ directions for the (0001) plane and parallel to the $[1\bar{1}00]$ and [0001] directions in the $(11\bar{2}0)$ plane. The critical aspect ratio for breakup into multiple pores, the kinetics of breakup, and the apparent surface diffusivity are affected by changes in channel crystallography. These behavioral differences are attributed to surface energy anisotropy effects.

This work was supported by the Director, the Office of Energy Research, Office of Basic Energy Sciences, Materials Sciences Division of the U. S. Department of Energy under Contract No. DE-AC03-76SF00098.

Introduction:

Surface diffusion may dominate coarsening of a compact during initial stage sintering, and/or may control the pore mobility during final stage sintering. Consequently, the absolute magnitude and temperature dependence of the surface diffusivity, D_s, and its magnitude and temperature dependence **relative** to that of competing transport mechanisms are important in describing and predicting microstructural evolution [1,2].

Results of experiments investigating crack healing [3,4], initial stage sintering [5-8], thermal grooving [9-11], scratch smoothing [12-14], and sintering [15] have been used to estimate absolute or relative values of D_s in alumina, and suggest a broad range of values. Differences in surface crystallography [13] and sample purity [9] are likely contributors to the variability.

The rates and characteristics of pore channel breakup can yield information on transport rates [16-18] and effects of surface energy anisotropy [19]. A recently introduced method for generating controlled-geometry interfacial pore arrays [20] provides a convenient method of studying the morphological evolution of pore channels. The method is particularly attractive because up to 10^6 features can be introduced on a single sample, channels can be etched into different planes and oriented along different directions within the plane, and the channel width and aspect ratio can easily be varied.

Theoretical background:

The morphological stability of continuous (cylindrical) phases has been a subject of interest since the first complete analysis of such

phenomena by Rayleigh [21]. The Rayleigh analysis predicts that infinitesimal periodic perturbations with a wavelength λ exceeding $2\pi r$ (the cylinder circumference) will reduce the surface energy per unit volume, and thus will increase in amplitude. Growth of perturbations with $\lambda > \lambda_{min}$ $(=2\pi r)$ eventually causes the formation of discrete particles (or pores) from an initially continuous phase.

For a cylindrical void with isotropic interfacial energy, both the perturbation growth rate and the magnitude of the kinetically dominant wavelength are predicted to depend on the dominant mass transport system [16]. Nichols and Mullins suggest the most rapidly growing wavelength will vary from $\sqrt{2}\cdot\lambda_{min}$ for surface diffusion dominated growth to $2.1\lambda_{min}$ for volume diffusion dominated growth. Intermediate values are predicted when both mechanisms contribute to breakdown.

Nichols examined the morphological stability of finite-length cylinders with hemispherical caps [18]. A critical length-to-diameter (L/D) ratio $\approx$7.2 is suggested, below which a single particle is formed (spheroidization), and above which breakup into two or more particles occurs.

Surface energy anisotropy modifies the behavior of both infinite and finite-length cylinders. Cahn evaluated the stability of single crystal rods with a specific surface energy (γ) isotropic in transverse (r-θ) planes, but a function of $\phi = (\partial r/\partial z)$, where z is the axial coordinate [19]. Surface energy anisotropy may have either a stabilizing or destabilizing effect. If the original surface orientation corresponds to a cusp in the γ versus ϕ plot, the cylinder is stabilized with respect to infinitesimal perturbations, however, may be unstable to finite perturbations. In contrast, when the original surface corresponds to a ridge in the γ - ϕ

plot, the cylinder is unstable. More generally, λ_{min} depends on the second derivative of γ with respect to ϕ. If $(\partial^2\gamma/\partial\phi^2)$ is positive (corresponding to minimum in γ at $\phi = 0$), λ_{min} is increased, and conversely.

Experimental method:

Pore structures were produced using procedures described previously [20]. Briefly, surface structures were generated on sapphire using photolithography and ion beam etching, and then transferred to an internal interface by hot pressing (1370°C, 60 min, 15 MPa, $2.6 \cdot 10^{-3}$ Pa) the patterned wafer to an unetched sapphire wafer.

Subsequently, the bonded samples were annealed under vacuum ($1.3 \cdot 10^{-3}$ Pa) for varying times at 1800°C. Structural evolution was monitored in two ways. The transparency of sapphire allows (nondestructive) observation of internal features using optical microscopy; samples could be given several heat treatments and characterized intermittently. Alternatively, the bicrystal could be split along the interface, and scanning electron microscopy used to characterize the interfacial pore structure.

Two pore patterns were used. Fig. 1a illustrates short channels of varying aspect ratio; pore widths were varied from 2.2 to 5.7 μm. Fig. 1b shows semi-infinite channels with widths of 2.2 to 7.7 μm; adjacent channel edges were spaced 20 μm apart to minimize interactions and transport between channels of differing size. Both types of patterns were etched into (0001) and $(11\bar{2}0)$ planes, and oriented parallel to the $[1\bar{1}00]$ and $[11\bar{2}0]$ directions for the (0001) plane and parallel to the $[1\bar{1}00]$ and [0001] directions in the $(11\bar{2}0)$ plane. Channel depths (measured by surface

profilometer) were 0.18 μm and 0.12 μm on the (0001) and $(11\bar{2}0)$ planes, respectively.

Etched crystals were bonded to unetched wafers of identical surface orientation, to produce bicrystals with twist angles <2°. After bonding and after annealing at 1800°C, pore areas in cross sections normal to the channel axes were measured from SEM micrographs. In both cases, the areas were identical to those calculated by multiplying the original channel width by the measured depth, indicating that the pores do not shrink.

During annealing at 1800°C, pore cross-sections became equiaxed, Fig. 2. Equilibration times were ≈20 and 10 min for channels in the (0001) and $(11\bar{2}0)$ planes, respectively. Internal pore structures could be imaged using visible light. Light is reflected back to the observer from channels in the (0001) plane, and away from the observer from channels in the $(11\bar{2}0)$ plane, causing equilibrated pores to appear light and dark, respectively. When using light microscopy, interference between reflections from the front and back faces of the pore channels led to color variations that correlated with axial variations in pore cross-section, thus providing additional information on the three-dimensional evolution of pore shape.

Data for the (0001) and $(11\bar{2}0)$ planes, were obtained from two samples of each orientation. For each orientation, >5000 200-μm long channels (Fig. 1b) and >10000 channels of variable aspect ratio (Fig. 1a) were contained in the interfaces. Additional experiments were conducted using 3000-μm long channels and other somewhat shorter channels.

Results:

Morphological evolution: The morphological evolution of a specific (0001)[$1\bar{1}00$]-oriented six-channel motif, following anneals of 0 to 200 min at 1800°C is presented in Figs. 3a-f. Several features characterized this and other similarly oriented pore arrays. Pore shape equilibration in the plane normal to the channel axis was rapid (Fig. 2). Channels shortened and developed end bulges prior to breakup. The distance over which the end bulge influenced the pore cross-section exceeded the wavelength of uniform perturbations that developed along the entire channel by a factor of 2 to 3. When and where pinchoff occurred, considerable readjustment of the end geometry ensued, leading to the development of a "longer wavelength" end bulge. Repeated pinchoff and readjustment produced an ultimate pore spacing substantially greater than the perturbation wavelength (node spacing) that developed along the channel. Pinchoff at numerous points along the channel, coupled with development of multiple end bulges, led to nonuniform pore sizes and spacings even for the uniform initial geometries studied. The spacing between adjacent cross-sectional minima (nodes) was measured in channels of differing widths. A total of 148 measurements were made; node spacings were between (7.3-13.9)·D, where D is the equivalent circular pore diameter. The spacing between 57 adjacent pores varied from (15.1-18.7)·D.

Results on finite aspect ratio channels were obtained from observations of the evolution of 40 pore arrays containing lower L/D channels of 1.0-μm diameter. Only 5% of the pores with L/D = 47 formed multiple pores, and only ≈15% of the highest L/D channels examined (78) evolved into two or more pores. This appears to be due to channel regression and end bulging similar to that in semi-infinite channels. Channel ends of 1.0-μm diameter

pores recede ≈25 μm, leaving only ≈28 μm of coarser channel available for pinchoff. In most cases, this was insufficient for formation of two pores.

Results obtained by fracturing the bicrystal and examining the interface using SEM are illustrated in Fig. 4. This particular figure shows channels 1 through 5 (top to bottom) with D = 1.1, 1.1, 0.9, 1.3, and 1.7 μm. Due to scaling law effects, the channels are at differing stages of evolution. Break-up of channel 3 is almost complete, channels 1 and 2 show the development of uniformly spaced maxima and minima along the channel, while nodes are less well developed in channels 4 and 5.

Although fewer (0001)[11$\bar{2}$0]-oriented channels have been studied, the results indicate that the channel direction within the basal plane affects the morphological evolution. Perturbations are much less pronounced, wavelengths are much longer, and the pore spacings evolved from 3000-μm long channels exceeded 110·D.

Changes in wafer orientation also produce significant changes in pore break-up behavior. Fig. 5a-c illustrate the evolution of channels etched parallel to the [0001] direction in the (11$\bar{2}$0) plane. As before, the channels rapidly became equiaxed in the transverse plane, ends receded and bulged, however, the perturbation form appears quite different from that for basal plane channels. Optical micrographs suggest that long thin pore channels connect bulged sections; the change in cross-section appears to be more step function like than sinusoidal. The number of bulged sections and nodes within a channel can change dramatically prior to pinchoff. While the nodes (145 measurements on different channels) have spacings between (19.4-27.2)·D, the final pores have spacings of (84.5-112.9)·D based on 109 measurements. When pore channels of lower variable aspect ratio (Fig. 1a)

were studied, only ≈10% of the highest aspect channels (L/D = 93) evolved into more than one pore (Table 1).

Channels with orientation $(11\bar{2}0)[1\bar{1}00]$ again demonstrate the importance of channel direction on morphological evolution, Fig. 6. A slight end bulge develops, however, no other minima or maxima appear to form along the channel (Fig. 6b). Pore pinchoff occurs primarily at the channel end, and thus, node and pore spacings are equal. Measurements of 263 pore spacings yielded values of 44.4-50.5·D. Only a small fraction of pore channels with L/D ≤ 93 evolved into more than one pore.

Table 1: Normalized perturbation characteristics as a function of orientation.

	$(0001)[1\bar{1}00]$	$(0001)[11\bar{2}0]$	$(11\bar{2}0)[0001]$	$(11\bar{2}0)[1\bar{1}00]$
(Node spacing)/D	7.3-13.9	--	19.4-27.2	44.4-50.5
(Pore spacing)/D	15.1-18.7	>100	84.5-112.9	44.4-50.5
Critical L/D	>78	--	>93	>93

Kinetics: To determine pinchoff times, samples were given multiple anneals with anneal time increments corresponding to ≈30% of the standard deviation for the average pinchoff time. The difficulties of determining meaningful surface diffusivities from this information are addressed, and "apparent" surface diffusion coefficients are reported.

For $[1\bar{1}00]$-oriented basal plane channels, the range of pinchoff times from three different interfaces was similar. Break-up times for nearly identical channels at different locations within the same bicrystal interface varied by up to a factor of 30. We attribute this variability to

effects of local variations in impurity content on D_s or the surface energy anisotropy [19], or possibly both.

Pinchoff time measurements for channels of $(11\bar{2}0)[0001]$ orientation were initially taken using a six-channel motif as illustrated in Fig. 1b. The wavelength for pinchoff was much larger than expected for an isotropic material, and thus only the ≈280 channels of higher aspect ratio (1-3) were used for measurements. Pinchoff times varied by a factor of ≈20 for channels of fixed D. A distribution of pinchoff times for channels of 0.72-μm diameter is shown in Fig. 7, and illustrates the strong variation in kinetics for channels of identical geometry and crystallography.

There are obvious difficulties in extracting surface diffusion coefficients from this data. Nichols [18] has proposed the following relationship between D_s and (initial) pinchoff times (t) for channels of equivalent radius r: $D_s \approx 3.67 \cdot [r^4/t] \cdot [kT/\gamma\Omega^2\nu]$. The model assumes isotropic surface energy, a circular cross-section, and a hemispherical end cap. The initially flat channels develop equiaxed equilibrium cross-sectional shapes after ≈2 to 5% of the average time required for pinchoff, however, the shape is not circular. The model predicts that the kinetically dominant wavelength for surface diffusion controlled perturbation growth is $\sqrt{2} \cdot \lambda_{min}$, which would lead to center-to center pore spacings of order $4.4 \cdot D$. Our measured spacings are ≈4 to 25 times larger. We believe that these differences reflect effects of surface energy anisotropy [19]. If average pinchoff times (at 1800°C) are <u>force-fit</u> into the expression for D_s, a surface diffusivity of $(1.7 \pm 1.0) \cdot 10^{-6}$ cm²/s is calculated for $(0001)[1\bar{1}00]$ channels, and $(1.05 \pm 0.53) \cdot 10^{-6}$ cm²/s is calculated for $(11\bar{2}0)[0001]$ channels. In view of the many discrepancies between the experimentally

observed and theoretically modelled geometries, comparisons of pinchoff times would be preferable and more meaningful.

An even more dramatic departure from isotropic behavior is provided by the $(11\bar{2}0)[1\bar{1}00]$ channels. Fig. 6 suggests that there is no systematic size dependence to the pinchoff time; times for >850 channels were recorded, and confirm this assertion. Possibly, perturbation growth involves a surface reaction rate limited step that overrides other size dependent effects. Further examination of this behavior is needed.

Discussion:

Striking differences exist between observed behavior and that predicted for isotropic materials. These differences manifest themselves in orientation dependent modes of evolution, and orientation dependent critical aspect ratios. Of the orientations examined, the behavior of $(0001)[1\bar{1}00]$ channels most closely approximates isotropic behavior. For the other orientations studied, the perturbation form does not appear to be sinusoidal. Furthermore, the critical aspect ratios for finite length channels and the final pore spacings for semi-infinite channels are much higher than expected for isotropic materials.

The differences in behavior between $(0001)[1\bar{1}00]$ and $(11\bar{2}0)[1\bar{1}00]$ channels are of particular interest since these channels have the same orientation; the grain boundaries for the two cases are simply orthogonal. This rather subtle difference apparently causes a significant difference in the morphological evolution; critical aspect ratios differ, as does the size dependence of the pinch-off time. We note that in Figs. 2e,f basal planes do not develop, whereas in Figs. 2c,d they do. Apparently, even

though the boundary misorientation is small (<2° twist), and the boundary energy is also small, it is sufficient to noticeably modify the equilibrium pore shape. The results then suggest that the grain boundary plane orientation is an important factor to consider in comparing the results from channels that have the same crystallographic orientation.

The results obtained indicate a wide spread in transport rates; one might question the significance of the data so derived. Our results show that crystallography accounts for at least some of the variability, and that factors such as channel direction and grain boundary plane orientation can be important variables, even at temperatures as high as 1800°C. Differences between observed trends (Table 1) and behavior expected for isotropic materials are widespread. Consequently, considerable caution should be exercised in use of analyses assuming isotropy. Furthermore, results and trends observed on one crystal orientation may only be valid for that orientation; generalization may be unwarranted. We have also seen changes in behavior that suggest a switch from surface diffusion controlled evolution to surface reaction rate limited evolution.

Even when channel crystallography and geometry are held constant, differences in evolution rates are seen. The relatively high spatial resolution of the technique, coupled with the ability to directly observe such a large number of events is believed to contribute to this spread. Other techniques in which the average behavior of many particles (sintering) or grain boundaries (grooving) of varying misorientation are studied would be less sensitive to changes in local environment (e.g., purity). Experiments comparing pinchoff times and distributions in doped and undoped crystals would be instructive.

As mentioned earlier, surface diffusion plays an important role in many kinetic processes of interest. Is the surface diffusion coefficient calculated from one set of experiments applicable to other processes, or are there important inherent differences in the surface transport processes? We have recently developed model experiments that allow studies of crack healing [22] and pore drag [23]. The crack healing measurements allow easy assessment of crack regression rates; we have observed rates as high as 7 nm/s. The pore drag experiments also provide information relative to grain coarsening processes in powder compacts. A comparison of the results may provide new insights.

Summary:

The morphological evolution of controlled geometry pore channels has been studied. The effects of surface crystallography, and channel geometry have been investigated. Effects of surface energy anisotropy on pore evolution are evident. Further experimental and theoretical work examining the effects of anisotropy and its impact on microstructural evolution is needed. Concurrently, further development and application of model experiments that directly examine the phenomena of interest is suggested.

References:

1. R. J. Brook; pp. 331-64 in Treatise on Materials Science and Technology, Vol. 9, Edited by F. F. Y. Wang, Academic Press, New York, 1976.
2. R. J. Brook, "Fabrication Principles for the Production of Ceramics with Superior Mechanical Properties," Proc. Br. Ceram. Soc., 32, 7-24 (1982).
3. C. F. Yen and R. L. Coble, "Spheroidization of Tubular Voids in Al_2O_3 Crystals at High Temperatures," ibid., 55, [10], 507-09 (1972).

4. T. K. Gupta, "Instability of Cylindrical Voids in Alumina," J. Am. Ceram. Soc., 61, [5-6], 191-95 (1978).
5. Y. Moriyoshi and W. Komatsu, "Kinetics of Initial Combined Sintering," Yogyo Kyokai Shi, 81, [3], 102-07 (1973).
6. S. Prochazka and R. L. Coble, "Surface Diffusion in the Initial Sintering of Alumina: I," Phys. Sint. 2, [1], 1-18 (1970); "II," ibid., [2] 1-14; "III," ibid., 15-34.
7. W. R. Rao and I. B. Cutler, "Initial Sintering and Surface Diffusion in Al_2O_3," J. Am. Ceram. Soc., 55, [3], 170-71 (1972).
8. P. Sajgalik, Z. Panek and M. Uhrik, "The surface diffusion coefficients of MgO and Al_2O_3," J. Mater. Sci., 22, [12], 4460-64 (1987).
9. W. M. Robertson and F. E. Ekstrom, "Impurity Effects in Surface DIffusion on Aluminum Oxide"; pp. 273-83 in Materials Science Research, Vol. 3, Edited by W. W. Kriegel and Hayne Palmour, III, Plenum, New York, 1966.
10. J. F. Shackelford and W. D. Scott, "Relative Energies of ($\bar{1}100$) Tilt Boundaries in Aluminum Oxide," 51, [12], 688-92 (1968).
11. A. R. Gaddipati and W. D. Scott, "Surface mass transport of alumina," J. Mater. Sci., 21, [2], 419-23 (1986).
12. T. Maruyama and W. Komatsu, "Surface Diffusion of Single Crystal Al_2O_3 by Scratch Smoothing Method," J. Am. Ceram. Soc., 58, [7-8], 338-9 (1975).
13. F. H. Huang, R. A. Henrichsen and C-Y. Li, pp. 173-186 in Sintering and Catalysis, Ed. G. C. Kuczynski, Plenum, New York, 1975.
14. C. Monty and J. Le Duigou, "The influence of the addition of MgO on the surface mass transport of alumina," High Temp.-High Pressures, 14, (1982).
15. K. A. Berry and M. P. Harmer, "Effect of MgO Solute on Microstructure Development in Al_2O_3," J. Am. Ceram. Soc., 69, [2], 143-49 (1986).
16. F. A. Nichols and W. W. Mullins, "Surface (Interface) and Volume-Diffusion Contributions to Morphological Changes Driven by Capillarity," Trans. A.I.M.E., 233, [10], 1840-48 (1965).
17. F. A. Nichols and W. W. Mullins, "Morphological Changes of a Surface of Revolution due to Capillarity-Induced Surface Diffusion," J. Appl. Phys., 36, [6], 1826-35 (1965).
18. F. A. Nichols, "On the Spheroidization of Rod-Shaped Particles of Finite Length," J. Mater. Sci., 11, [6], 1077-82 (1976).
19. J. W. Cahn, "Stability of Rods with Anisotropic Surface Free Energy," Scripta Metall., 13, [11], 1069-71 (1979).
20. J. Rödel and A. M. Glaeser, "Production of Controlled Morphology Intergranular Pore Arrays: Implications and Opportunities," J. Am. Ceram. Soc., 70, [8], C172-C175 (1987).
21. Lord Rayleigh, "On the Instability of Jets," Proc. London Math. Soc., 10, 4-13 (1879).
22. J. Rödel and A. M. Glaeser, "Application of controlled interfacial pore structures to kinetic studies in alumina," to appear in Interfacial Structures, Properties and Design, (Mater. Res. Soc. Proc., 122, Pittsburgh, PA 1988); (also LBL Report #25010).
23. J. Rödel and A. M. Glaeser, "Pore Drag in Alumina," this volume.

Figure Captions:

Figure 1: SEM micrographs of: (a) pores of constant width but varying L/D, and (b) semi-infinite channels of varying width.

Figure 2: SEM micrographs of cross-sections taken normal to the channel axis: (a,b) after etching and bonding, (c,d) after 20 min at 1800°C for channels in the (0001) plane, and (e,f) after 10 min at 1800°C for channels in the $(11\bar{2}0)$ plane.

Figure 3: The morphological evolution of a specific $(0001)[1\bar{1}00]$ oriented six-channel motif, following anneals of (a) 0, (b) 40, (c) 60, (d) 90, (e) 135, and (f) 200 min at 1800°C.

Figure 4: SEM micrograph of bicrystal fracture surface with 5-channel array. Channels 1 through 5 (top to bottom) have diameters of 1.1, 1.1, 0.9, 1.3, and 1.7 μm, respectively. Sample was annealed for 25 h at 1800°C.

Figure 5: $(11\bar{2}0)[0001]$-oriented pore channels after: (a) bonding, (b) $7\frac{1}{2}$ h, and (c) 48 h at 1800°C.

Figure 6: $(11\bar{2}0)[1\bar{1}00]$-oriented pore channels after: (a) 5 min, (b) $1\frac{1}{2}$ h, (c) 5 h, and (d) 48 h at 1800°C.

Figure 7: Incremental percentage of $(11\bar{2}0)[0001]$-oriented, 0.72-μm diameter pore channels exhibiting pinchoff versus total anneal time at 1800°C.

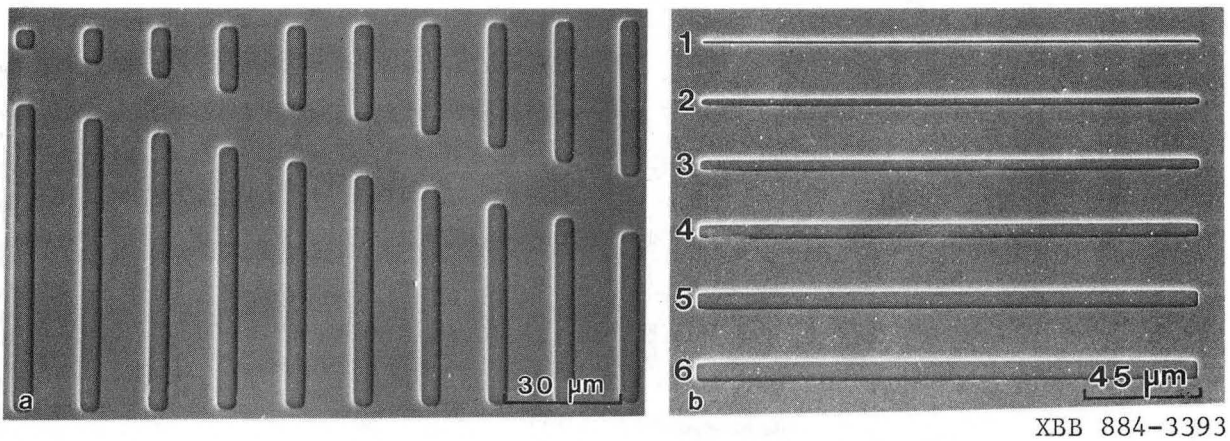

XBB 884-3393

Fig. 1

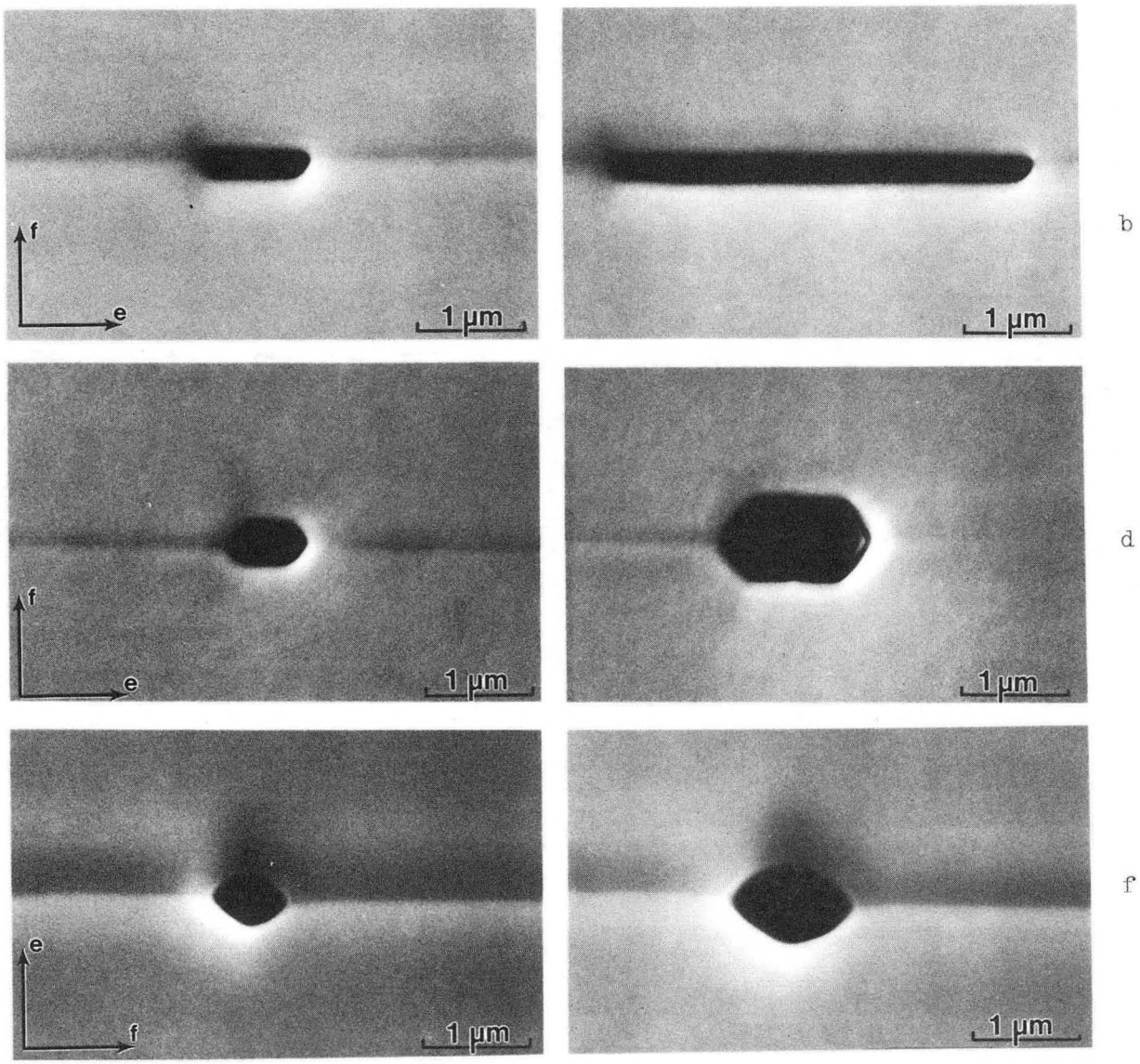

XBB 884-3387

Fig. 2

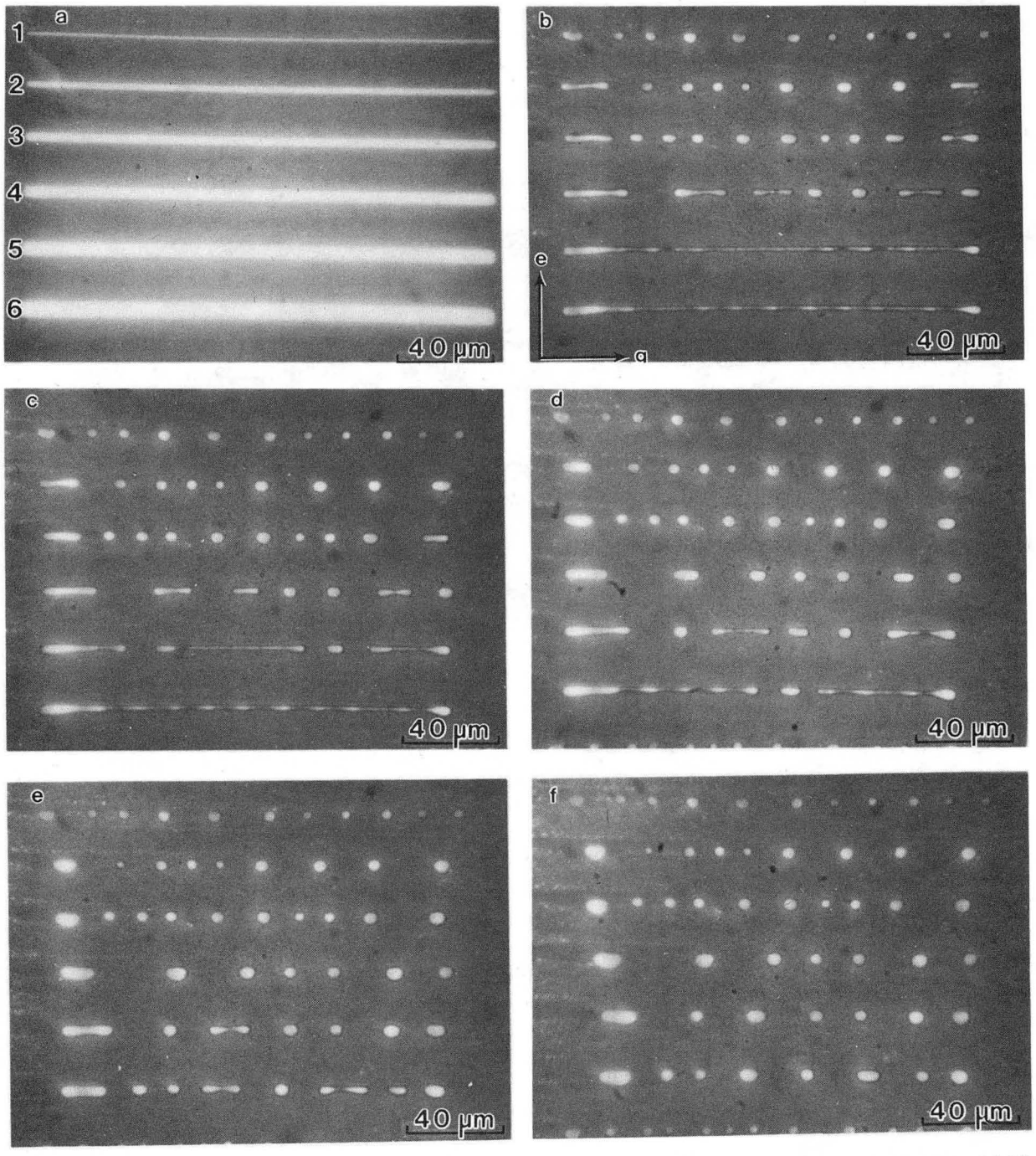

XBB 884-3391

Fig. 3

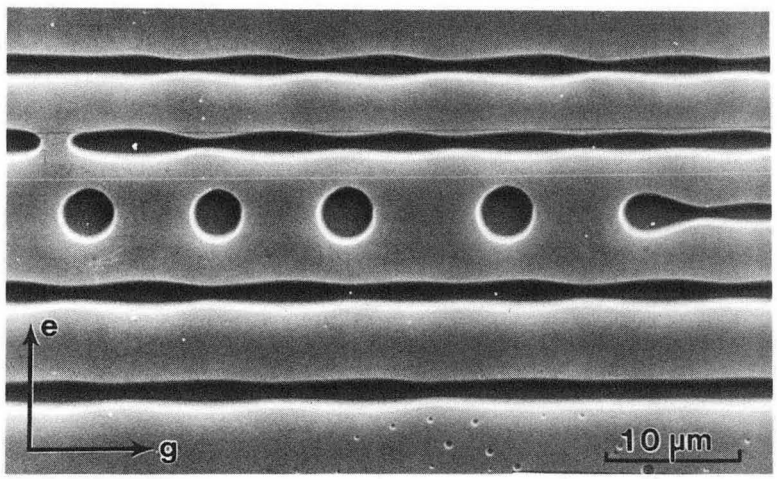

XBB 884-3395

Fig. 4

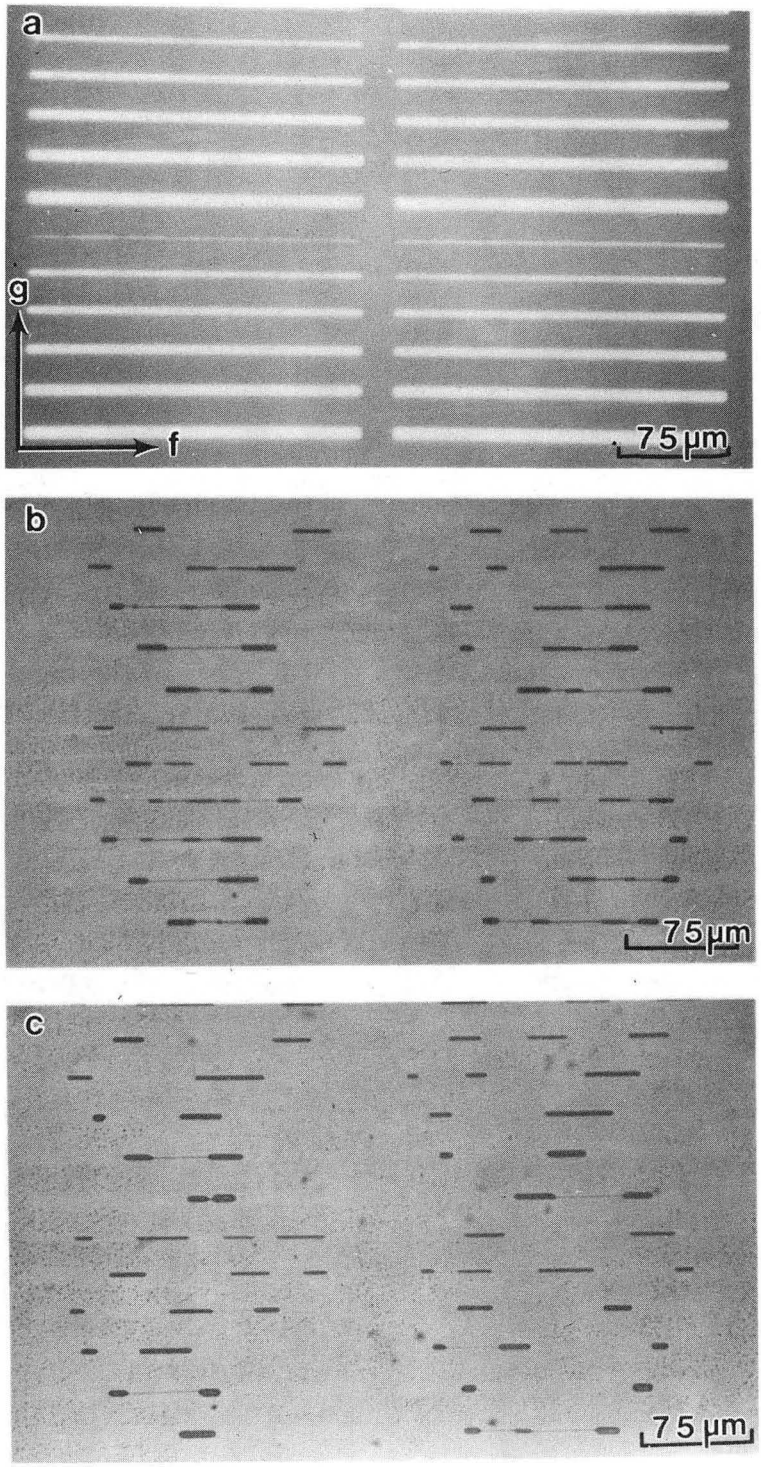

XBB 884-3394

Fig. 5

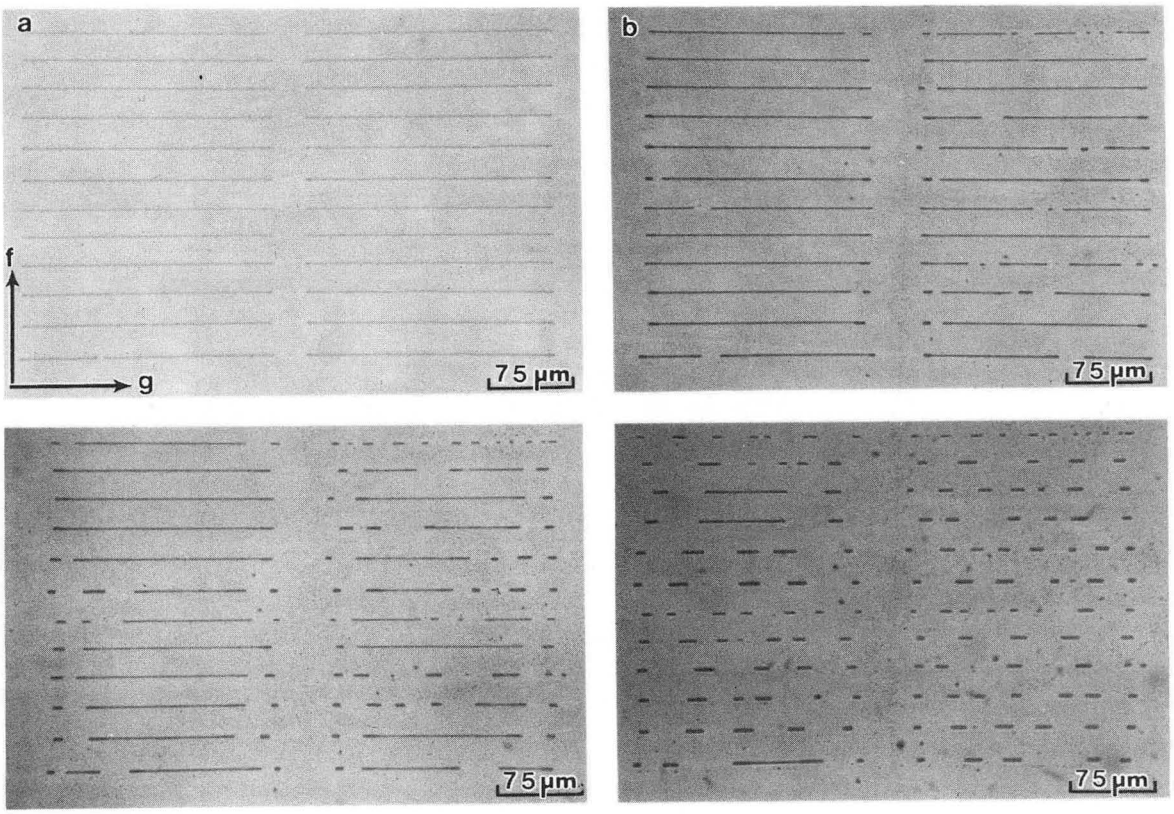

XBB 884-3390

Fig. 6

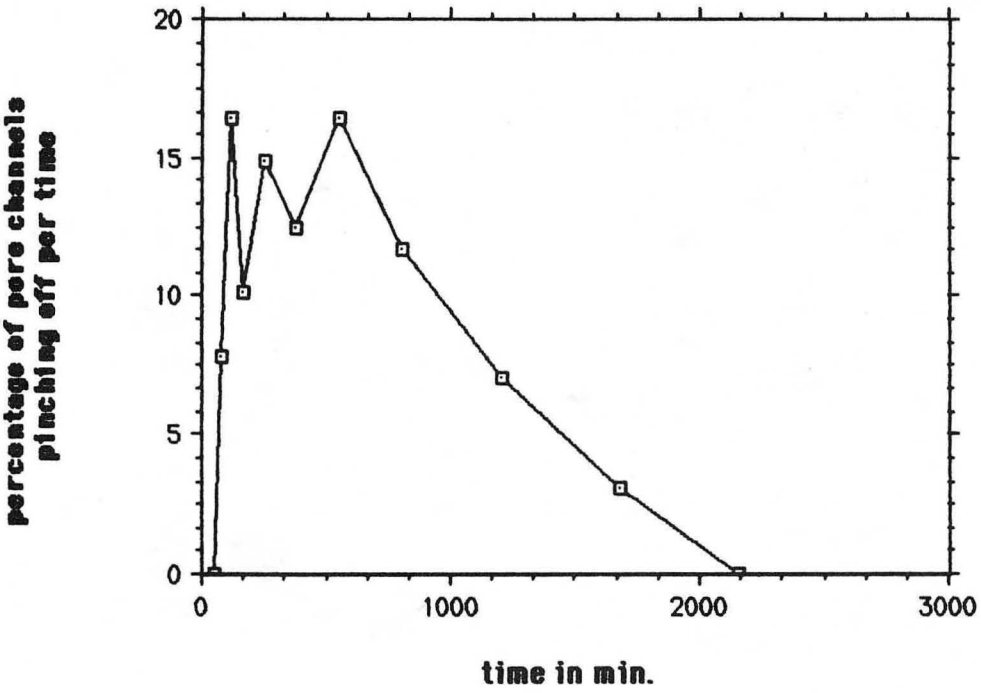

XBL 885-1570

Fig. 7

LAWRENCE BERKELEY LABORATORY
TECHNICAL INFORMATION DEPARTMENT
UNIVERSITY OF CALIFORNIA
BERKELEY, CALIFORNIA 94720